# Direct measurement of coherent phonon dynamics in solution-processed stibnite thin films

Wee Kiang Chong,[1,2,*] Guichuan Xing,[1,3,*] Yun Liu,[4] Ee Ling Gui,[5] Qing Zhang,[1] Qihua Xiong,[1,3,6] Nripan Mathews,[3,5] Chee Kwan Gan,[4,†] and Tze Chien Sum[1,3,‡]

[1]*Division of Physics and Applied Physics, School of Physical and Mathematical Sciences, Nanyang Technological University, 21 Nanyang Link, Singapore 637371*

[2]*Energy Research Institute @NTU (ERI@N), Interdisciplinary Graduate School, Research Techno Plaza, X-Frontier Block, Level 5, 50 Nanyang Drive, Singapore 637553*

[3]*Singapore-Berkeley Research Initiative for Sustainable Energy, 1 Create Way, Singapore 138602, Singapore*

[4]*Institute of High Performance Computing, 1 Fusionopolis Way, #16-16 Connexis, Singapore 138632*

[5]*School of Materials Science and Engineering, Nanyang Technological University, Nanyang Avenue, Singapore 639798*

[6]*NOVITAS, Nanoelectronics Center of Excellence, School of Electrical and Electronic Engineering, Nanyang Technological University, Singapore 639798*

(Received 17 April 2014; revised manuscript received 1 July 2014; published 23 July 2014)

We report observations of coherent phonon oscillations in solution-processed polycrystalline stibnite ($Sb_2S_3$) photovoltaic thin films using transient absorption spectroscopy. Detailed optical spectroscopy correlated by extensive first-principles lattice dynamics calculations indicates that the coherent $B_{3g}$ longitudinal optical phonon mode with a frequency of 63.74 ± 0.05 $cm^{-1}$ (or 1.911 ± 0.002 THz) at room temperature is generated via the impulsive stimulated-Raman-scattering mechanism. These strong electron-phonon interactions indicate a dominant energy-loss channel in these materials that could impose a fundamental limit on their solar energy conversion efficiency.

DOI: 10.1103/PhysRevB.90.035208 PACS number(s): 72.15.Jf, 63.20.kd, 78.47.jb, 78.30.−j

Stibnite or antimony sulfide ($Sb_2S_3$), which belongs to the metal chalcogenide family, is a technologically important compound semiconductor due to its excellent optical and thermoelectric properties [1,2]. Given its small direct band gap, large absorption coefficient ($\alpha > 5 \times 10^4$ $cm^{-1}$) in the visible region, low toxicity, and earth-abundant elemental composition [3], there has been a recent surge of interest into utilizing it as a low-cost solution-processable light absorber layer for solid-state semiconductor-sensitized solar cells [4–7]; power conversion efficiencies as high as 6.3% have been reported [4]. Despite these promising traits, detractors have been skeptical of whether this semiconductor system could be further improved [8]. Although device engineering and materials optimization are important routes to realizing highly efficient photovoltaic devices, it is also essential to examine the intrinsic properties, which cannot be truly controlled via improved fabrication. Unfortunately, basic studies into its fundamental properties such as dynamical electron-phonon interactions are few and far between. Such intrinsic properties arising from the motion of the valence electrons in the crystal and their coupling with the lattice have a profound influence on the electronic and thermoelectric properties, which in turn have considerable impact on device operations. The insights gained from a clear understanding of these lattice dynamics would shed light on the suitability of $Sb_2S_3$ as an absorber layer for solar energy conversion.

Herein, we examine the coherent phonon dynamics in solution-processed $Sb_2S_3$ photovoltaic thin films using transient absorption spectroscopy and correlate the findings with Raman spectroscopy and first-principles lattice dynamics calculations. Femtosecond laser pulses with duration shorter than the phonon period are ideal probes for investigating oscillatory phenomena in single-crystalline thin films and superlattices [9–12]. Our findings reveal the generation of a coherent $B_{3g}$ longitudinal optical phonon mode with a frequency of 63.74 ± 0.05 $cm^{-1}$ (or 1.911 ± 0.002 THz) at room temperature by ultrafast pulses through the impulsive stimulated-Raman-scattering (ISRS) mechanism. These coherent phonon oscillations at room temperatures are observed in solution-processed polycrystalline $Sb_2S_3$ thin films [3]. Typically, such phonon oscillations have only been observed in single crystals or single-crystalline thin films or superlattices, with the $A_{1g}$ mode, exhibiting displacive behavior [9–12].

Our samples comprise chemical-bath-deposited $Sb_2S_3$ films of ∼100 nm grown directly on FTO substrate (control) and four different multilayered thin-film samples with a configuration FTO/$TiO_2$/$Al_2O_3$/$Sb_2S_3$—typical of photovoltaic devices. Chemical-bath deposition of $Sb_2S_3$ is performed by immersing the FTO substrate in a mixture of solutions comprising 650 mg of antimony chloride ($SbCl_3$) dissolved in 2.5 mL of acetone $(CH_3)_2CO$, 3.950 g of sodium thiosulfate ($Na_2S_2O_3$) in 25.0 mL of de-ionized (DI) water, and 72.5 mL of DI water for 1 h at 4 °C. Thin films of $Sb_2S_3$ films are then annealed at 330 °C in argon flow for 30 min. The $TiO_2$ and $Al_2O_3$ layers in the multilayered FTO/$TiO_2$/$Al_2O_3$/$Sb_2S_3$ samples were grown by spray pyrolysis and plasma atomic-layer deposition (ALD), respectively. Dense $TiO_2$ blocking layers were deposited using homemade spray pyrolysis of titanium (IV) bis(acetylacetonate)-di(isopropanoxylate) (TAA) on FTO and subsequently converted into $TiO_2$ by annealing at 450 °C in ambient conditions. Thin $Al_2O_3$ layers were grown on top of $TiO_2$ using plasma ALD at 200 °C with trimethylaluminum (TMA) and $O_2$ plasma as precursors. The thickness of the $Al_2O_3$ layer was varied by

*These authors contributed equally to this work.
†Corresponding author: ganck@ihpc.a-star.edu.sg
‡Corresponding author: tzechien@ntu.edu.sg

 

controlling the ALD deposition cycles (i.e., two, five, seven, ten cycles), where a thickness of 1.1 Å is estimated for each cycle.

Room-temperature femtosecond transient absorption spectroscopy (TAS) was performed using a standard two-color pump-probe setup. The laser pulses (150 fs, 800 nm) were generated from a 1 kHz Coherent Legend regenerative amplifier that was seeded by a 80 MHz Coherent Vitesse Ti:sapphire oscillator. The 400-nm (3.1-eV) pump beam was generated by frequency doubling the 800-nm output from the regenerative amplifier using a beta-barium borate (BBO) crystal, while the white light continuum probe (450–800 nm) was generated by focusing a small portion (~5 $\mu$J) of the fundamental 800-nm laser pulses into a 2-mm-thick sapphire plate. The 400-nm pump excitation is resonant with one of the absorption peaks of the $Sb_2S_3$ samples—see Fig. 1 for the linear absorption spectrum where $Sb_2S_3$ has a direct band gap of 1.62 eV. The desired probe wavelength is then selected using a spectrometer. The pump and probe pulses were cross polarized to eliminate any contribution from coherent artifacts at early times. Pump-induced changes in transmission ($\Delta T$) of the probe beam were monitored using a standard monochromator–photomultiplier tube configuration with lock-in detection. $\Delta T$ can be expressed using the equation

$$\Delta T \approx T_e + \frac{\partial T}{\partial \chi}\frac{\partial \chi}{\partial Q}Q, \tag{1}$$

where $T_e$ represents the electronic contributions, and the second term with the Raman tensor $\frac{\partial \chi}{\partial Q}$ represents the oscillatory contribution. The second term approximates the phonon dynamics using first-order Taylor expansion of $\Delta T$ in terms of lattice displacement $Q$. As such, only Raman-active modes with nonzero Raman tensor can be detected by the lock-in amplifier. The pump beam was chopped at 83 Hz and this was used as the reference frequency for the lock-in amplifier.

Raman-scattering spectroscopy was carried out at room temperature to compare the frequencies of the Raman-active modes with the frequency of the oscillations obtained from TAS. The measurement was performed using a micro-Raman spectrometer (Horiba-JY T64000) equipped with a liquid nitrogen cooled charge-coupled device and conducted in a backscattering configuration excited with a solid-state green laser ($\lambda = 532$ nm). The backscattered signal was collected through a 100 × objective and dispersed by a 1800 g/mm grating under a triple subtractive mode with a spectra resolution of 1 $cm^{-1}$ and ~5 $cm^{-1}$ limit of detection.

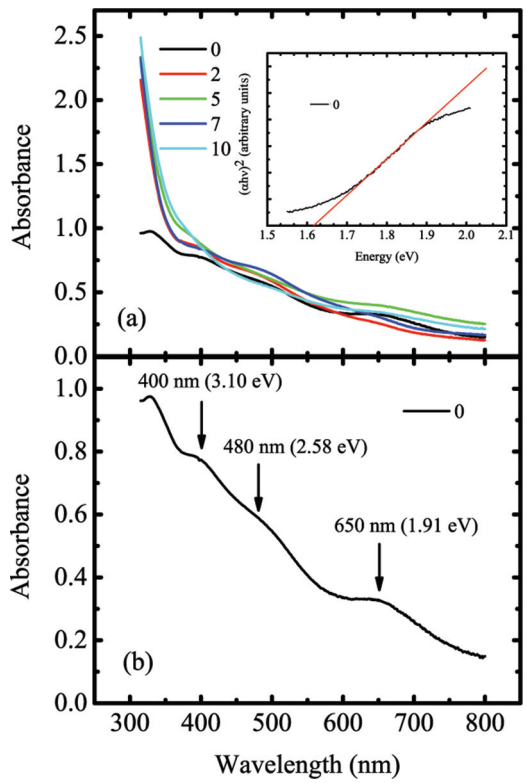


FIG. 1. (Color online) (a) Steady-state absorption of the five samples. 0 refers to FTO/$Sb_2S_3$ while 2, 5, 7, 10 refers to the samples with $Al_2O_3$ grown using different ALD cycles. Inset shows the Tauc plot for $Sb_2S_3$ with its direct band gap shown by the $x$ intercept. (b) Steady-state absorption spectrum of $Sb_2S_3$. The labeled peaks represent the dominant energy transitions in the prepared $Sb_2S_3$.

Figure 1 shows the steady-state absorption spectra of the samples. From the figure, there appears to be no significant absorption change among the samples above 400 nm. This is consistent with the band gap of the materials since only $Sb_2S_3$ can be excited above this wavelength. For allowed direct transition, a Tauc plot has shown the band gap of $Sb_2S_3$ to be 1.62 ± 0.03 eV [inset of Fig. 1(a)]. In addition, as shown in Fig. 1(b), three absorption peaks were observed for $Sb_2S_3$ at ~400, 480, and 650 nm. These peak positions are close to the reported values in the literature [13] and they correspond predominantly to the sulfur 3$p$ to antimony 5$p$ transitions [14]. These transitions are possible due to wave-function admixing between the two orbitals [15].

Figure 2(a) shows the broadband transient absorption (TA) spectra (420–780 nm) for the FTO/$TiO_2$/$Al_2O_3$(10 ALD cycles)/$Sb_2S_3$ sample at different probe delays following pump excitation at 400 nm (3.1 eV) with a pump fluence of 6.37 $\mu J/cm^2$. Following photoexcitation, these hot carriers will then redistribute the energy through coherent phonon generation, electron-phonon coupling, carrier diffusion, and electron-hole recombination. The TA kinetics at 570-nm wavelength in Fig. 2(b) shows a damping oscillatory component superimposed on the nonoscillatory photoinduced absorption (PIA) (i.e., negative $\Delta T/T$) component. As shown in Fig. 2(c), with increasing $Al_2O_3$ layer thickness, the oscillations become more prominent. The presence of the oscillations even in FTO/$Sb_2S_3$ clearly shows that the oscillations originate directly from $Sb_2S_3$ layer.

Figure 3 shows the TA data for the same FTO/$TiO_2$/$Al_2O_3$(10 ALD cycles)/$Sb_2S_3$ sample at different probe wavelengths. The oscillatory behavior is evident across the entire probe wavelength range. The PIA component originates from the excitation of the hot carriers to even higher energy levels by the probe beam which is described by a multiexponential decaying function. Thermalization

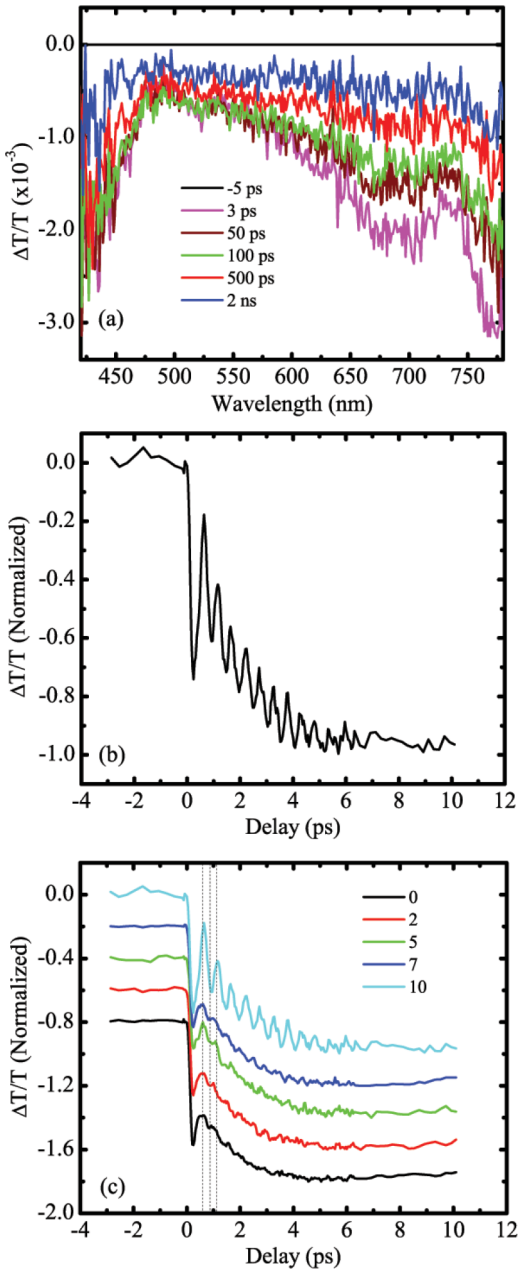


FIG. 2. (Color online) (a) White light transient absorption (TA) spectrum (420–780 nm) of FTO/$TiO_2$/$Al_2O_3$(10 ALD cycles)/$Sb_2S_3$ at various time delays following pump excitation. (b) Normalized PIA ($-\Delta T/T$) transient kinetics at 570-nm probe wavelength extracted from the white light TA spectrum. (c) Normalized TAS temporal spectrum of the pure $Sb_2S_3$ film on (0) on FTO and the four multilayered films (2, 5, 7, 10—labeled according to the ALD cycles) probed at 570 nm (pump fluence = 6.37 $\mu$J/cm$^2$). The dotted lines are guides to the eyes to show that the samples exhibit similar oscillating frequencies.

of the hot carriers through electron-phonon coupling and carrier diffusion contribute to the decay process. The damping oscillatory component, on the other hand, can be described by the following equation:

$$-\Delta T = A\cos(2\pi f t + \varphi)\exp\left(\frac{-t}{\tau}\right), \qquad (2)$$

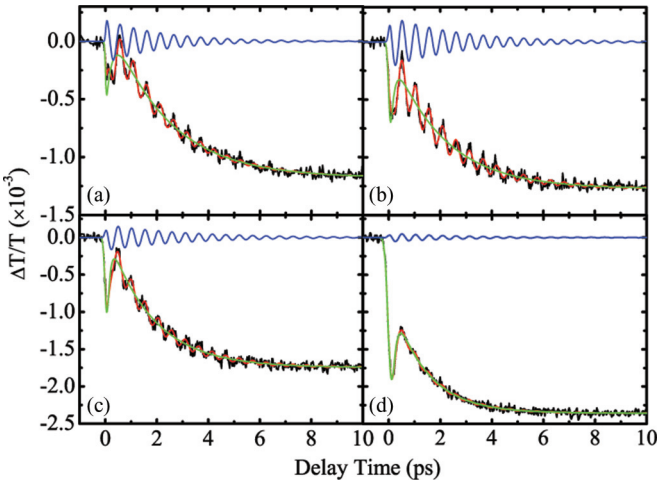


FIG. 3. (Color online) (a) Probe wavelength dependent study of FTO/$TiO_2$/$Al_2O_3$(10 ALD cycles)/$Sb_2S_3$ (pump intensity = 6.37 $\mu$J/cm$^2$) at wavelength (a) 450 nm, (b) 550 nm, and (c) 650 nm and (d) 750 nm. Green, blue, and red lines in (a)–(d) represent the fitting of electronic signal, oscillatory signal, and total signal, respectively. The fitted frequencies are (a) 63.91 cm$^{-1}$, (b) 63.61 cm$^{-1}$, (c) 63.81 cm$^{-1}$, and (d) 63.64 cm$^{-1}$.

where $A$ is the oscillatory amplitude, $f$ is the phonon frequency, $\varphi$ is the oscillation phase, and $\tau$ is the phonon lifetime. The respective transients were fitted by overlaying the oscillatory component on a multiexponential decaying function. The average deconvolved frequency was found to be 63.74 $\pm$ 0.05 cm$^{-1}$ (or 1.911 $\pm$ 0.002 THz) in all cases with a small average cosine phase of 0.0 $\pm$ 0.1 rad.

Possible origins of these coherent oscillations include (a) multiple probe reflections off the sample interfaces which would exhibit sample thickness and probe wavelength dependence in the oscillation period; (b) probe beams reflected off acoustic waves in $Sb_2S_3$ generated by the pump pulse which would exhibit probe wavelength dependence in the oscillation period; and (c) phonon oscillations generated by the femtosecond laser pulses. For (a), under favorable interference conditions, multiple probe beams reflected off interfaces with different thicknesses could give rise to probe oscillations. As such interference conditions are dependent on the layer thickness, the oscillation period from such interactions should also vary with layer thickness. However, the invariance of the oscillation period with overall sample thickness suggests that multiple probe reflections are unlikely to be the origin of these oscillations [Fig. 1(c)]. The invariance of the oscillation period for different probe wavelengths further eliminates the conclusions for case (a) and also similarly discounts case (b) for probe beams reflected off acoustic waves as a possible origin of these oscillations. As such, we attribute these coherent oscillations to originate from phonons [case (c)].

The generation of coherent phonon oscillations in materials could arise from two different mechanisms: (i) impulsive stimulated Raman scattering (ISRS) or (ii) displacive excitation of coherent phonon (DECP). These mechanisms can be described using the classical analogs of how oscillations may be generated in a pendulum system [16]; in (i) the pendulum

is set to oscillate by initially displacing the pendulum while in (ii) the pendulum is set to oscillate by initially displacing the pivot. The oscillations from (i) arise from the excitation of phonons due to the energy difference between two components in a broad energy spectral pulse; while those from (ii) arise from the shifting of potential energy surfaces of the system from its equilibrium as a result of carrier excitation into the conduction band. Resonant energy excitation conditions would excite cosine-type oscillations while nonresonant excitation would lead to sine-type oscillations. Unlike ISRS where both oscillation types are possible, only symmetrical modes (i.e., $A_1/A_g/A_{1g}$) with cosine oscillations are expected from excitations arising from the DECP mechanism [12]. Although the DECP mechanism was originally believed to be distinct, it was later found by Merlin *et al.* that it is in fact a special case of resonant ISRS for optically absorbing (opaque) materials [17,18]. To establish the excitation mechanism responsible for these coherent phonon oscillations in our $Sb_2S_3$ thin films, steady-state Raman spectroscopy was also performed to determine the frequencies of the Raman-active modes (Fig. 4). Out of 60 phonon modes from $Sb_2S_3$ with $D_{2h}$ symmetry at Γ, only 30 optical phonon modes are Raman active (under the *Pnma* convention: $10A_g+5B_{1g}+10B_{2g}+5B_{3g}$). Figure 4 shows the Raman spectrum for the $Sb_2S_3$/quartz sample fitted with multiple Lorentzian peaks. Out of 60 phonon modes from $Sb_2S_3$ with $D_{2h}$ symmetry (30 are Raman active under the *Pnma* convention: $10A_g+5B_{1g}+10B_{2g}+5B_{3g}$), as many as 11 Raman modes are found from the fit of the Raman spectrum (Fig. 4) and tabulated in Table I.

Density functional theory calculations as implemented in the QUANTUM ESPRESSO suite [19] using the Perdew-Burke-Ernzerhof-type (PBE) exchange correlation functional were performed to gain a deeper insight into the physical origins of the Raman modes. $Sb_2S_3$ has an orthorhombic crystal structure consisting of parallel one-dimensional ($Sb_4S_6$) ribbons (Fig. 5). To account for the inter-ribbon dispersive forces, we employed the semiempirical dispersion corrections (Dispersion-corrected Density Functional Theory version 2 (DFTD2)) proposed by Grimme [20]. The phonon frequencies were calculated using density functional perturbation theory [21,22]. Norm-conserving pseudopotentials were generated using the QUANTUM ESPRESSO "atomic" code under the scheme of Rappe-Rabe-Kaxiras-Joannopoulos [23]. Electronic wave functions were expanded in plane-wave basis sets with energy cutoff of 60 Ry. The unit cell structure is optimized with residual forces of less than $10^{-3}$ eV/Å and stresses of less than $10^{-4}$ eV/Å$^3$. A $3 \times 9 \times 3$ Monkhorst-Pack $k$-point grid is used for the Brillouin zone integration. These experimental values correlate well with our calculated frequencies and literature values [24] as summarized in Table I. Our calculations revealed two closely separated phonon modes, $B_{3g}$ and $B_{1g}$, with frequencies 64.96 and 64.86 cm$^{-1}$, respectively; both are in very good agreement with the oscillation frequency 63.74 ± 0.05 cm$^{-1}$ obtained from TAS. As nonresonant

TABLE I. A comparison of the Raman data in this work with our calculations and those values from the literature. Only zone center modes with frequencies close to the Raman values are listed.

| Raman mode | This work (cm$^{-1}$) | Our calculations (cm$^{-1}$) | Literature [24] (cm$^{-1}$) |
|---|---|---|---|
| $B_{1g}$ | 36.80 | 44.79 | 43 |
| $A_g$ | 50.60 | 51.63 | 51 |
| $B_{3g}$ | 60.19 | 64.96 | – |
| $A_g$ | 72.13 | 74.22 | 72 |
| $B_{2g}$ | 95.48 | 90.55 | – |
| $B_{2g}$ | 123.89 | 121.26 | – |
| $A_g$ | 158.26 | 165.63 | 156 |
| $B_{2g}$ | 194.39 | 191.90 | – |
| $B_{1g}$ | 240.79 | 228.60 | 239 |
| $A_g$ | 282.71 | 279.22 | 283 |
| $A_g$ | 309.42 | 295.56 | 312 |

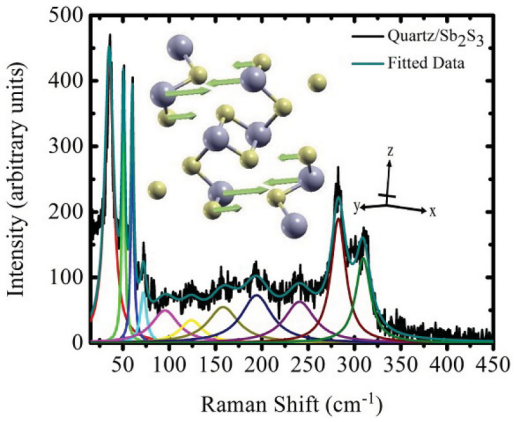


FIG. 4. (Color online) Steady-state Raman spectrum using 532-nm CW laser source of 0.06 mW and 100 × objective lens. Inset: The representative vibration of the $B_{3g} = 64.96$ cm$^{-1}$ phonon mode with S atoms shown in yellow and Sb in purple. The atoms oscillate along the $y$ axis, parallel to the ribbons. The image is rendered using XCRYSDEN [31].

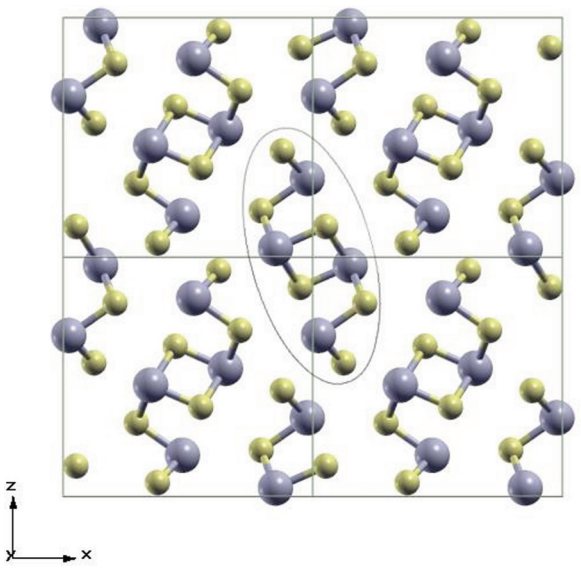


FIG. 5. (Color online) Ball-and-stick model of four primitive cells of $Sb_2S_3$ with S atoms shown in yellow and Sb in purple. The perspective is along the $y$ axis, and one $Sb_4S_6$ ribbon is circled out. The image is rendered using XCRYSDEN [31].

TABLE II. Comparison between the calculated lattice parameter and coherent phonon modes with experimental values. The bracket indicates the nonresonant Raman-scattering coefficient in units of Å$^4$/amu using LDA [25].

| | Experiment [32] | PBE+Grimme |
|---|---|---|
| $a$/Å | 11.311 | 11.430 |
| $b$/Å | 3.836 | 3.888 |
| $c$/Å | 11.223 | 10.964 |
| $B_{1g}$/cm$^{-1}$ | | 64.86 (2.0) |
| $B_{3g}$/cm$^{-1}$ | | 64.96 (1140) |

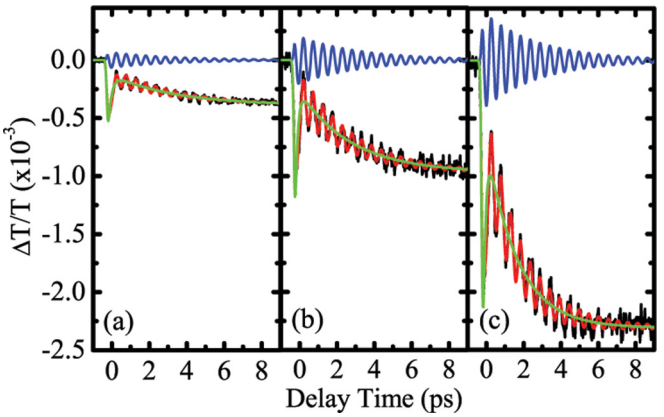


FIG. 6. (Color online) Pump fluence study of FTO/$TiO_2$/$Sb_2S_3$ (10 ALD cycles) probed at 570 nm at fluence (a) 3.18 $\mu$J/cm$^2$, (b) 6.37 $\mu$J/cm$^2$, and (c) 12.7 $\mu$J/cm$^2$ wavelength. Green, blue, and red lines in (a)–(c) represent the fitting of electronic signal, oscillatory signal, and total signal, respectively. The fitted frequencies are (a) 63.64 cm$^{-1}$, (b) 63.94 cm$^{-1}$, and (c) 63.71 cm$^{-1}$.

Raman coefficients calculations have been implemented in QUANTUM ESPRESSO for the local density approximation (LDA) functional but not the PBE functional we relied on the LDA for a determination of the nonresonant coefficients [25] where we expect they should not sensitively depend on the functional choice. Table II shows that the $B_{1g}$ mode has a negligible coefficient—indicating that it is not likely to be excited in the experiments. On the other hand, the $B_{3g}$ mode (Fig. 5 inset) has a much higher cross section, making it a more likely candidate.

We will also need to consider the possibility of phonon softening of the $A_g$ Raman mode at from 74.22 cm$^{-1}$ to 63.74 cm$^{-1}$. Phonon softening was previously observed in materials such as Bi [26] and Te [27,28]. This effect occurs when a large density of carriers is excited under high pump fluence leading to a lower phonon frequency being observed from TAS. However, in our TA experiments, the photoexcited carrier density at the highest pump fluence of 15.9 $\mu$J/cm$^2$ is very small (i.e.,<0.01% of excited valence electrons—estimated based on number of valence electrons excited per $Sb_2S_3$ unit cell)—indicating that lattice weakening is very unlikely to have taken place. Furthermore, the first-principles calculations (where the effects of electronic excitation are incorporated using the Fermi-Dirac distribution [29,30]) reveal that under a photoexcited carrier density of <0.01%, the frequencies of all phonon modes only softened by an order of 0.1 cm$^{-1}$. Further evidence that phonon softening is insignificant can be obtained from the pump fluence dependent TAS measurements (Fig. 6) where the oscillation frequencies remain invariant over the range of 3.18–12.7 $\mu$J/cm$^2$. Hence, the optical phonon mode with $B_{3g}$ symmetry can be identified with the oscillations found from TAS. Since this mode has been deduced to be nonsymmetrical, a displacive type of excitation could therefore be ruled out. Lastly, it is also important to show that the mode is not initiated by the relaxation of carriers. This is evident from the small extracted cosine phase of 0.0 ± 0.1 rad which corresponds to a time delay of 0 ± 80 fs. From the electronic signal ($T_e$) in Fig. 2(b), the hot charge carrier cooling time can be estimated to be a few picoseconds. This is longer than the time delay of 0 ± 80 fs and implies that the mode cannot be initiated by carrier cooling. On the other hand, the 80 fs time scale correlates well with half the temporal width of the pump pulse (150 fs). This implies that the mode is likely to be generated from the laser pulse. Although it is also possible for phonons to be excited via energy matching from two separate components from a pump and probe pulse when they overlap at time zero (0 ps delay), this scenario could also be ruled out since the frequency remains invariant with probe wavelength as shown in Fig. 3. Hence, we believe that the coherent phonon oscillations observed originate from an ISRS excitation mechanism solely initiated by the pump pulse. Our findings contrast with the $A_{1g}$ mode found in single-crystalline $Bi_2Te_3$, $Sb_2Te_3$ thin films or superlattices, exhibiting displacive behavior [9–12].

In summary, coherent phonon dynamics in solution-processed $Sb_2S_3$ photovoltaic thin films was generated and probed using transient absorption spectroscopy. Raman measurements in conjunction with theoretical calculations showed that the coherent optical phonon mode possesses $B_{3g}$ symmetry. Our findings reveal that this mode originates from an ISRS excitation mechanism initiated by the pump pulse. These findings of dominant electron-phonon interactions shed light on an effective energy-loss channel through phonon relaxation that could impose a fundamental limit on the efficiency of $Sb_2S_3$ as a photovoltaic material, but on the other hand it is highly desirable for thermoelectric applications.

T.C.S. acknowledges support from the following research grants: NTU start-up Grant No. M4080514), SPMS collaborative Research Award No. M4080536), Ministry of Education (MOE) Academic Research Fund (AcRF) Tier 2 Grant No. MOE2013-T2-1-081, and the Competitive Research Programme (CRP) grant under Project No. NRF-CRP5-2009-04. N.M. acknowledges support from NTU start-up Grant No. M4081293. Q.X. acknowledges support of this work from the Singapore National Research Foundation through NRF fellowship Grant No. NRF-RF2009-06 and Competitive Research Program Grant No. NRF-CRP-6-2010-2, Ministry of Education AcRF Tier 2 Grants No. MOE2011-T2-2-051 and No. MOE2012-T2-2-086 and start-up grant support (Grant No. M58113004) from Nanyang Technological University (NTU). Q.X., N.M., and T.C.S. also acknowledge financial support from the

Singapore National Research Foundation through the Singapore-Berkeley Research Initiative for Sustainable Energy (SinBerRISE) CREATE Programme. Y.L. acknowledges support from National Science Scholarship, Singapore, and also A*STAR Computational Resource Centre through the use of its high-performance computing facilities.

[1] B. Roy, B. R. Chakraborty, R. Bhattacharya, and A. K. Dutta, Solid State Commun. **25**, 937 (1978).
[2] L. P. Deshmukh, S. G. Holikatti, B. P. Rane, B. M. More, and P. P. Hankare, J. Electrochem. Soc. **141**, 1779 (1994).
[3] E. L. Gui, A. M. Kang, S. S. Pramana, N. Yantara, N. Mathews, and S. Mhaisalkar, J. Electrochem. Soc. **159**, B247 (2012).
[4] J. A. Chang, S. H. Im, Y. H. Lee, H. J. Kim, C. S. Lim, J. H. Heo, and S. I. Seok, Nano Lett. **12**, 1863 (2012).
[5] S. H. Im, C. S. Lim, J. A. Chang, Y. H. Lee, N. Maiti, H. J. Kim, M. K. Nazeeruddin, M. Gratzel, and S. I. Seok, Nano Lett. **11**, 4789 (2011).
[6] Y. Itzhaik, O. Niitsoo, M. Page, and G. Hodes, J. Phys. Chem. C **113**, 4254 (2009).
[7] C. S. Lim, S. H. Im, J. H. Rhee, Y. H. Lee, H. J. Kim, N. Maiti, Y. Kang, J. A. Chang, M. K. Nazeeruddin, M. Gratzel, and S. I. Seok, J. Mater. Chem. **22**, 1107 (2012).
[8] A. Darga, D. Mencaraglia, C. Longeaud, T. J. Savenije, B. O'Regan, S. Bourdais, T. Muto, B. Delatouche, and G. Dennler, J. Phys. Chem. C **117**, 20525 (2013).
[9] T. K. Cheng, J. Vidal, H. J. Zeiger, G. Dresselhaus, M. S. Dresselhaus, and E. P. Ippen, Appl. Phys. Lett. **59**, 1923 (1991).
[10] Y. G. Wang, X. F. Xu, and R. Venkatasubramanian, Appl. Phys. Lett. **93**, 113114 (2008).
[11] A. Q. Wu, X. Xu, and R. Venkatasubramanian, Appl. Phys. Lett. **92**, 011108 (2008).
[12] H. J. Zeiger, J. Vidal, T. K. Cheng, E. P. Ippen, G. Dresselhaus, and M. S. Dresselhaus, Phys. Rev. B **45**, 768 (1992).
[13] S. D. Shutov, V. V. Sobolev, Y. V. Popov, and S. N. Shestatskii, Phys. Status Solidi B **31**, K23 (1969).
[14] T. Ben Nasr, H. Maghraoui-Meherzi, H. Ben Abdallah, and R. Bennaceur, Phys. B: Condens. Matter **406**, 287 (2011).
[15] A. V. Powell, R. J. E. Lees, and A. M. Chippindale, J. Phys. Chem. Solids **69**, 1000 (2008).
[16] K. Ishioka and O. V. Misochko, in *Progress in Ultrafast Intense Laser Science* (Springer, Berlin, 2010), pp. 23–46.
[17] G. A. Garrett, T. F. Albrecht, J. F. Whitaker, and R. Merlin, Phys. Rev. Lett. **77**, 3661 (1996).
[18] T. E. Stevens, J. Kuhl, and R. Merlin, Phys. Rev. B **65**, 144304 (2002).
[19] P. Giannozzi, S. Baroni, N. Bonini, M. Calandra, R. Car, C. Cavazzoni, D. Ceresoli, G. L. Chiarotti, M. Cococcioni, I. Dabo, A. Dal Corso, S. de Gironcoli, S. Fabris, G. Fratesi, R. Gebauer, U. Gerstmann, C. Gougoussis, A. Kokalj, M. Lazzeri, L. Martin-Samos *et al.*, J. Phys.: Condens. Matter **21**, 395502 (2009).
[20] S. Grimme, J. Comput. Chem. **25**, 1463 (2004).
[21] S. Baroni, S. de Gironcoli, A. Dal Corso, and P. Giannozzi, Rev. Mod. Phys. **73**, 515 (2001).
[22] P. Giannozzi, S. de Gironcoli, P. Pavone, and S. Baroni, Phys. Rev. B **43**, 7231 (1991).
[23] A. M. Rappe, K. M. Rabe, E. Kaxiras, and J. D. Joannopoulos, Phys. Rev. B **41**, 1227 (1990).
[24] P. Sereni, M. Musso, P. Knoll, P. Blaha, K. Schwarz, and G. Schmidt, in *XXII International Conference on Raman Spectroscopy*, AIP Conf. Proc. No. 1267, edited by P. M. Champion and L. D. Ziegler (AIP, Melville, NY, 2010), pp. 1131–1132.
[25] Y. Liu, K. T. E. Chua, T. C. Sum, and C. K. Gan, Phys. Chem. Chem. Phys. **16**, 345 (2014).
[26] M. Hase, M. Kitajima, S.-i. Nakashima, and K. Mizoguchi, Phys. Rev. Lett. **88**, 067401 (2002).
[27] S. Hunsche, K. Wienecke, T. Dekorsy, and H. Kurz, Phys. Rev. Lett. **75**, 1815 (1995).
[28] S. Hunsche, K. Wienecke, and H. Kurz, Appl. Phys. A **62**, 499 (1996).
[29] V. Recoules, J. Clerouin, G. Zerah, P. M. Anglade, and S. Mazevet, Phys. Rev. Lett. **96**, 055503 (2006).
[30] P. B. Hillyard, D. A. Reis, and K. J. Gaffney, Phys. Rev. B **77**, 195213 (2008).
[31] A. Kokalj, Comput. Mater. Sci. **28**, 155 (2003).
[32] P. Bayliss and W. Nowacki, Z. Kristallogr. – Cryst. Mater. **135**, 308 (1972).